Nuclear Instruments and Methods in Physics Research B 365 (2015) 371–375

Contents lists available at ScienceDirect

Nuclear Instruments and Methods in Physics Research B

journal homepage: www.elsevier.com/locate/nimb

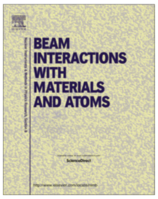

BEAM
INTERACTIONS
WITH
MATERIALS
AND ATOMS

Modifications of structural and physical properties induced by swift heavy ions in $Gd_2Ti_2O_7$ and $Y_2Ti_2O_7$ pyrochlores

N. Sellami [a,*], G. Sattonnay [a], C. Grygiel [b], I. Monnet [b], A. Debelle [c], C. Legros [a], D. Menut [d], S. Miro [e], P. Simon [f], J.L Bechade [d], L. Thomé [c]

[a] Univ. Paris Sud, ICMMO-LEMHE, Bât. 410, F-91405 Orsay, France
[b] CIMAP, CEA, CNRS, Université de Caen, BP 5133, F-14070 Caen Cedex 5, France
[c] CSNSM, CNRS, IN2P3, Université Paris-Sud, Bât. 108, F- 91405 Orsay, France
[d] CEA, DEN, Service de Recherches Métallurgiques Appliquées, 91191 Gif-Sur-Yvette, France
[e] CEA, DEN, Service de Recherches de Métallurgie Physique, Laboratoire JANNUS, F-91191 Gif-sur-Yvette, France
[f] CNRS UPR 3079 CEMHTI, 1D avenue de la Recherche Scientifique, F-45071 Orléans Cedex 2, France

ARTICLE INFO

Article history:
Received 29 September 2014
Received in revised form 30 April 2015
Accepted 8 July 2015
Available online 25 July 2015

Keywords:
Ion irradiation
Pyrochlores
X-ray diffraction
Raman spectroscopy

ABSTRACT

The structural transformations induced by ionization processes in $Gd_2Ti_2O_7$ and $Y_2Ti_2O_7$ pyrochlores irradiated with swift heavy ions have been studied using XRD and Raman experiments. Results show that irradiation induces amorphization and that the phase transformation build-up can be accounted for in the framework of a model involving a single-impact mechanism. The radiation induced amorphization build-up is faster in $Gd_2Ti_2O_7$ than in $Y_2Ti_2O_7$. Moreover, a decrease of the thermal conductivity (measured by the laser flash method) is induced by irradiation both in $Gd_2Ti_2O_7$ and $Y_2Ti_2O_7$.

1. Introduction

Pyrochlore-based oxides with the $A_2B_2O_7$ stoichiometry provide a large array of technologically important properties with potential applications such as solid oxide fuel cells [1] or host materials for actinide immobilization [2,3]. $Y_2Ti_2O_7$ is an important compound of this oxide family with a high ionic conductivity [4]. Moreover, nanoparticles of $Y_2Ti_2O_7$ pyrochlore were recently identified in oxide dispersion strengthened (ODS) steels as reinforcing oxides into the steel matrix [5]. Since ODS are potential candidates as cladding materials in future nuclear reactors, the structural stability of $Y_2Ti_2O_7$ under irradiation must be investigated.

Pyrochlores of formula $A_2B_2O_6O'$ are superstructures (Fd $\bar{3}$ m space group) of the fluorite structure (Fm $\bar{3}$ m space group) with two cation sites: larger cations are incorporated in the eight-coordinate A-site, whereas smaller cations occupy the six-coordinate B-site. Oxygen atoms are located in two anions sites O (48f) and O′ (8b). Concerning the effects of ion-irradiation in pyrochlores, it is well established that the susceptibility to radiation-induced amorphization in these compounds is related to their chemical composition [6–21]: whatever the ion energy range, rare earth titanates (for instance $Gd_2Ti_2O_7$) undergo a pyrochlore to amorphous transition, whereas most of rare earth zirconates (for instance $Gd_2Zr_2O_7$) are transformed into an anion-defect fluorite structure. Nevertheless, for some rare earth zirconates, the phase transformation induced by irradiation depends on the ion energy: in the nuclear collision regime (i.e. from few keV to few MeV) $Nd_2Zr_2O_7$ undergoes a pyrochlore to fluorite transition, whereas it is amorphized by the electronic excitation arising from swift heavy ion slowing down [22]. Recently, a few studies have been undertaken to understand the behavior of pyrochlores under irradiation with very energetic heavy ions [14–23] without only few results concerning $Y_2Ti_2O_7$ [24].

This paper reports a study, using X-ray diffraction (XRD), Raman spectroscopy and thermal diffusivity measurements, of the damage created by swift heavy ions in titanates (essentially $Y_2Ti_2O_7$ and $Gd_2Ti_2O_7$) in order to investigate the effects of electronic excitation on:

(i) The nature of the phases induced by irradiation and the kinetics of phase transitions;
(ii) The thermal conductivity of the materials.

---

* Corresponding author. Tel.: +33 1 69 15 70 37.
E-mail address: neila.sellami@u-psud.fr (N. Sellami).

http://dx.doi.org/10.1016/j.nimb.2015.07.017
0168-583X/© 2015 Elsevier B.V. All rights reserved.

2. Experimental

Polycrystalline pyrochlore pellets of YTO ($Y_2Ti_2O_7$) and GTO ($Gd_2Ti_2O_7$) were prepared by a standard solid state process. Stoichiometric amounts of A_2O_3 (with A = Y, Gd) and TiO_2 oxides were intimately mixed in an acetone slurry using a ball-mill and subsequently dried. After drying, the powders were isostatically pressed into rods at 250 MPa. The homogenized mixtures were then subjected to a three step heating protocol with intermittent grindings to attain a better homogeneity. The compacts were first sintered at 1200 °C for 12 h. The procedures (grinding, milling, pressing) were repeated twice with a second heating at 1400 °C for 72 h and a final sintering in air at 1450 °C for 196 h. Pellets were cut with a diamond saw and the specimens were polished to a 0.5 µm diamond finish.

Samples were irradiated at room temperature with 92-MeV Xe ions at the GANIL accelerator in Caen (IRRSUD beamline) at fluences ranging from 2×10^{15} up to $2 \times 10^{20}\ m^{-2}$. The ion flux was always kept lower than $10^9\ cm^{-2}s^{-1}$ in order to keep target heating less than 50 °C. Table 1 gives the projected range (R_p), as well as the nuclear (S_n) and electronic (S_e) stopping powers, calculated with the SRIM code [25] for YTO and GTO. These data show that S_e is higher than S_n by several orders of magnitude. Therefore the effects of electronic excitation are specifically investigated in this study.

XRD analysis were performed with a X'pert Pro MRD PANalytical diffractometer at the ICMMO-SP2M in Orsay, using a $Cu_{K\alpha}$ anticathode ($\lambda_{K\alpha1} = 0.1540598$ nm, $\lambda_{K\alpha2} = 0.1544426$ nm). X-ray patterns were recorded from 13° to 65° (2θ) with a step of 0.025°, with a grazing incidence of 2°. Complementary XRD analysis was done at the CEA Saclay/DEN/SRMA using a Bruker D8 Advance setup in asymmetric geometry. A conventional line focus Cu–Kα radiation is collimated with a parabolic Göbel mirror and a knife at the exit is used to suppress the Cu–Kβ line contribution. Axial divergence (i.e. in the plane perpendicular to the diffraction plane) is reduced to 1.5° with the use of longue Soller slits. The diffracted beam is collected by a one-dimensional Vantec detector without energy discrimination used. The sample is mounted on a motorized goniometric head, and rocking-curves are performed to align the sample along the incident beams. Due to the mean-grain size that was about few hundreds micrometres (observed by scanning electron microscopy), samples were spinned and further, precession effects were corrected. With this asymmetric setup, no diffusion vector out of the place defined by the incident beam and the normal to the surface of the sample. XDR patterns were recorded from 10 to 140° (2θ) with a step of 0.028° and a fixed incident angle of 2°. In this latter case, a maximum depth of ≈1 µm is analysed.

Raman characterizations were done with a Renishaw Invia Reflex device equipped with a Leica DM2500 microscope (×100 objective) at the JANNUS laboratory in Saclay. Raman scattering measurements were performed using the 532 nm line of a frequency-doubled Nd-YAG laser with an output power of around 2 mW to avoid sample heating. The maximum analysed depth is ≈10 µm.

The thermal diffusivity of samples, D_{th}, was measured from 20 °C to 630 °C using a laser-flash apparatus (Netzsch LFA 427) operating in an argon gas atmosphere. A laser pulse heats one side of a plane-parallel sample. The temperature rise on the backside due to the energy input is time-dependent detected. The specimen dimensions were Φ 8 mm × (1–2) mm of thickness. The thermal conductivity (λ) of the specimen was calculated using the following equation:

$$\lambda = D_{th}\rho C_p \tag{1}$$

where ρ is the density and C_p is the specific heat capacity. The samples densities were measured using the Archimede method. The heat capacities were estimated according to the Neumann–Kopp rule using the Gd_2O_3, Y_2O_3 and TiO_2 heat capacity values from a thermodynamic database. Because the sintered specimens were not fully dense, the measured thermal conductivities were corrected using the method proposed by Lutique et al. [26]:

$$\lambda = \lambda_0(1 - \phi)^{1.7} \tag{2}$$

where Φ is the fractional porosity. The relative density of elaborated samples is given in Table 1.

Table 1
Relative density, ion projected range (R_p), nuclear (S_n) and electronic (S_e) energy losses calculated with the SRIM code [23] for 92 MeV-Xe ions in $Gd_2Ti_2O_7$ and $Y_2Ti_2O_7$.

Compounds	Relative density (%)	R_p (µm)	S_e (keV/nm)*	S_n (keV/nm)*
$Gd_2Ti_2O_7$	99	7.6	22.1	0.4
$Y_2Ti_2O_7$	97	7.9	20.8	0.4

* Values computed at the surface of samples.

3. Results and discussion

3.1. Structural modifications

Fig. 1 shows diffraction patterns recorded on polycrystalline YTO and GTO pellets before and after irradiation with 92-MeV Xe ions. A progressive vanishing of the (222) peak is observed for both compounds and an additional diffuse scattering occurs at the basis of this peak. This broad peak arises from the diffuse scattering due to the formation of an amorphous phase. Finally, only the diffuse peak is observed at a fluence of $10^{17}\ m^{-2}$ and $5 \times 10^{16}\ m^{-2}$ for YTO and GTO respectively.

The amorphous fraction, A for each fluence, was deduced from the net areas of the corresponding XRD lines by using the equation:

$$A = 1 - \frac{\sum_{i=1}^{n} \frac{S_i^{irradiated}}{S_i^{unirradiated}}}{n} \tag{3}$$

where $S_i^{irradiated}$ and $S_i^{unirradiated}$ are the net areas of the i^{th} XRD line in the patterns recorded on irradiated and unirradiated samples, respectively, and n is the number of lines considered. Pseudo-Voigt profiles were used to fit the diffraction peaks. Fig. 2 presents the variation *versus* the ion fluence of the amorphous fractions extracted from XRD results according to the analysis procedure described above, for YTO and GTO irradiated with 92 MeV Xe ions. The data show that amorphization is almost complete at $5 \times 10^{16}\ m^{-2}$ for $Gd_2Ti_2O_7$ and at $10^{17}\ m^{-2}$ for YTO. The rate of amorphization is higher for GTO than for YTO, indicating that GTO is less resistant to radiation-induced disordering than YTO.

Phase transformation build-ups similar to those exhibited in Fig. 2 are generally accounted for in the framework of a single impact model [27]. In this model, the phase transformation is produced by an ion impinging into an undamaged region (only one impact is sufficient to totally transform the matter inside the ion track), the overall damage observed at high fluence resulting from the overlapping of a large number of ion tracks. Thus, the variation of the transformed fraction (f) with the ion fluence follows the simple equation [27]:

$$f = f_{sat}[1 - exp(-\sigma\phi)] \tag{4}$$

where f_{sat} is the transformed fraction at saturation (i.e. at very high fluence), σ is the section of the cylinder surrounding the ion path in which the transformation occurred, and ϕ is the ion fluence.

The amorphization build-up obtained for ion irradiations performed in this work were fitted with Eq. (4) (see solid lines in